Journal of Magnetic Resonance 349 (2023) 107404

Contents lists available at ScienceDirect

Journal of Magnetic Resonance

journal homepage: www.elsevier.com/locate/jmr

# Windowed cross polarization at 55 kHz magic-angle spinning

Evgeny Nimerovsky *, Stefan Becker, Loren B. Andreas *

*Department of NMR based Structural Biology, Max Planck Institute for Multidisciplinary Sciences, Am Fassberg 11, Göttingen, Germany*

ARTICLE INFO

*Article history:*
Received 6 January 2023
Revised 1 February 2023
Accepted 10 February 2023
Available online 16 February 2023

*Keywords:*
Magic-Angle Spinning NMR
Windowed Cross Polarization
FLAN conditions

ABSTRACT

Cross polarization (CP) transfers via Hartmann-Hahn matching conditions are one of the cornerstones of solid-state magic-angle spinning NMR experiments. Here we investigate a windowed sequence for cross polarization (wCP) at 55 kHz magic-angle spinning, placing one window (and one pulse) per rotor period on one or both rf channels. The wCP sequence is known to have additional matching conditions. We observe a striking similarity between wCP and CP transfer conditions when considering the flip angle of the pulse rather than the rf-field strength applied during the pulse. Using fictitious spin-1/2 formalism and average Hamiltonian theory, we derive an analytical approximation that matches these observed transfer conditions. We recorded data at spectrometers with different external magnetic fields up to 1200 MHz, for strong and weak heteronuclear dipolar couplings. These transfers, and even the selectivity of CP were again found to relate to flip angle (average nutation).



## 1. Introduction

Cross polarization (CP) transfer between heteronuclear spins [1–2] is a fundamental building block of multidimensional magic-angle spinning (MAS) NMR experiments. The spatial dependence of the dipolar interaction between a pair of spins allows not only to enhance the low gamma spin signals via CP, but also to quantitatively determine the dipolar coupling in materials and biological samples [3–15]. The combination of dipolar cross polarization transfer experiments with ultra-fast MAS probes [16–19] and proton detection [20–24] is an efficient tool for chemical shift assignments and structure determinations of the investigated samples [25–27] CP is also central to dynamic nuclear polarization spectroscopy [28–29], which enables characterization of compounds at lower spin concentration or in much less experimental time [30–32].

Hartmann-Hahn conditions [1] for MAS NMR can be efficient for both zero-quantum (ZQ) and double-quantum (DQ) conditions [33–36]. They occur, respectively, when the difference or the sum of the simultaneously applied nutation frequencies (rf-field strengths) matches the rotor frequency or twice the rotor frequency:

$$ZQ: \nu_I - \nu_S = n_{ZQ}\nu_R \qquad DQ: \nu_I + \nu_S = n_{DQ}\nu_R \tag{1}$$

where $\nu_I$ and $\nu_S$ are applied rf-field strengths on I and S spins, respectively; $\nu_R$ is a MAS rate and $n_{ZQ}, n_{DQ}$=±1,±2. Eq. (1) describes the Hartmann-Hahn conditions for CP transfers between a pair of spins. Hartmann-Hahn conditions can also be simultaneously achieved for two different heteronuclear pairs. [37–38].

While the CP transfer experiment defined by Eq. (1) has a constant power [39], called single-amplitude CP (SA-CP), better transfer efficiency can typically be reached with variable-amplitude CP [40]. Metz et al. [41] proposed a ramped-amplitude CP experiment with a linear amplitude ramp, which is commonly used. In 1995, Hediger et al. [42] demonstrated polarization transfer with an adiabatic passage through Hartmann-Hahn conditions. Additional variations were developed around the Hartmann-Hahn conditions by modulating not only the amplitude, but also the phase or the offset of the applied pulses to decrease the rf-field power mismatches and the offset dependence [43–58]. Methods based on optimal control [59–60], symmetry-based recoupling [61], multiple-contact [62–63], or longitudinal transfer [45,64], have also been proposed as alternative transfer elements. Some robust methods are based on different mechanisms [65–67], where the rf-field strengths and phases are optimized using optimal control algorithms [59–60,68] or they consist of trains of hard pulses with specific phase cycling [61,64,69].

In 1993 Hediger et al. [70] investigated amplitude-modulated cross-polarization [71–73] (AMCP) schemes for improvement of polarization transfer characteristics for MAS rates of 5 to 7 kHz. Using a sample of adamantane, it was shown that the AMCP sequences can help broaden CP conditions. One of the schemes, S-AMCP, initially proposed by Barbara and Williams [72], con-

* Corresponding authors.
*E-mail addresses:* evni@mpinat.mpg.de (E. Nimerovsky), land@mpinat.mpg.de (L.B. Andreas).

https://doi.org/10.1016/j.jmr.2023.107404
1090-7807/

tained a CW-spin lock pulse on one of the channels and rotor synchronized windowed rf-field on the other. At 5–7 kHz, this windowed sequence (wCP) resulted in improved transfer at n = 0, but ineffective spin lock, leading to relaxation. Here, we explore this sequence, as well as an extension of if with windows on both channels, at 55 kHz. The rotor period is then about 10 times shorter than in previous work, which can be expected to result in more efficient transfer due to a more effective spin lock. This motivates revisiting this sequence on modern NMR spectrometers at 600 to 1200 MHz where wCP might become a more competitive heteronuclear transfer element. In addition, it motivates the theoretical reconsideration and reanalysis with simplified definition of the optimal condition.

In this article we investigate windowed cross polarization (wCP), in which windowed rf-field is applied on one or both channels, without phase alternation. We analyze the wCP sequence with respect to the pulse flip angle values and derive optimal FLip ANgle conditions (FLAN) under which zero-quantum (ZQ) and double-quantum (DQ) transitions are observed. We provide theoretical, numerical and experimental analysis of the transferred signals with CP and wCP and show the connection between Hartmann-Hahn and FLAN conditions. For most cases wCP demonstrates similar efficiency as CP. We find that a windowed version of spectrally induced filtering in combination with cross polarization (SPECIFIC-CP) [44] can provide more efficient transfers, which is demonstrated with lipid bilayer samples of the membrane protein Influenza A M2 using 55.555 kHz MAS.

## 2. Result and discussion

Fig. 1A shows the wCP pulse sequence, where a single pulse with a window every rotor period is applied on at least one channel. The wCP sequence was proposed along with other AMCP sequences by Barbara and Williams [72] in 1992 and investigated by Hediger et al. [70] in 1993. The arrangement of the windowed pulses can also be different, for example, a pair of pulses with a single window between them. However, we find that these two approaches provide the same efficiency. While in simulations and experiments we applied both approaches (see the supplemental information), for simplicity, the following considers only the pulse sequence shown in Fig. 1A.

In this work we apply a well-known approach using fictitious spin-1/2 formalism [74] and average Hamiltonian theory (AHT) [75]. Note that Floquet formalism provides an alternate approach to simulation of AMCP sequences as intensively investigated by Hediger et al in 1993 [70], 1995 [76] and 1997 [77], and Nielsen

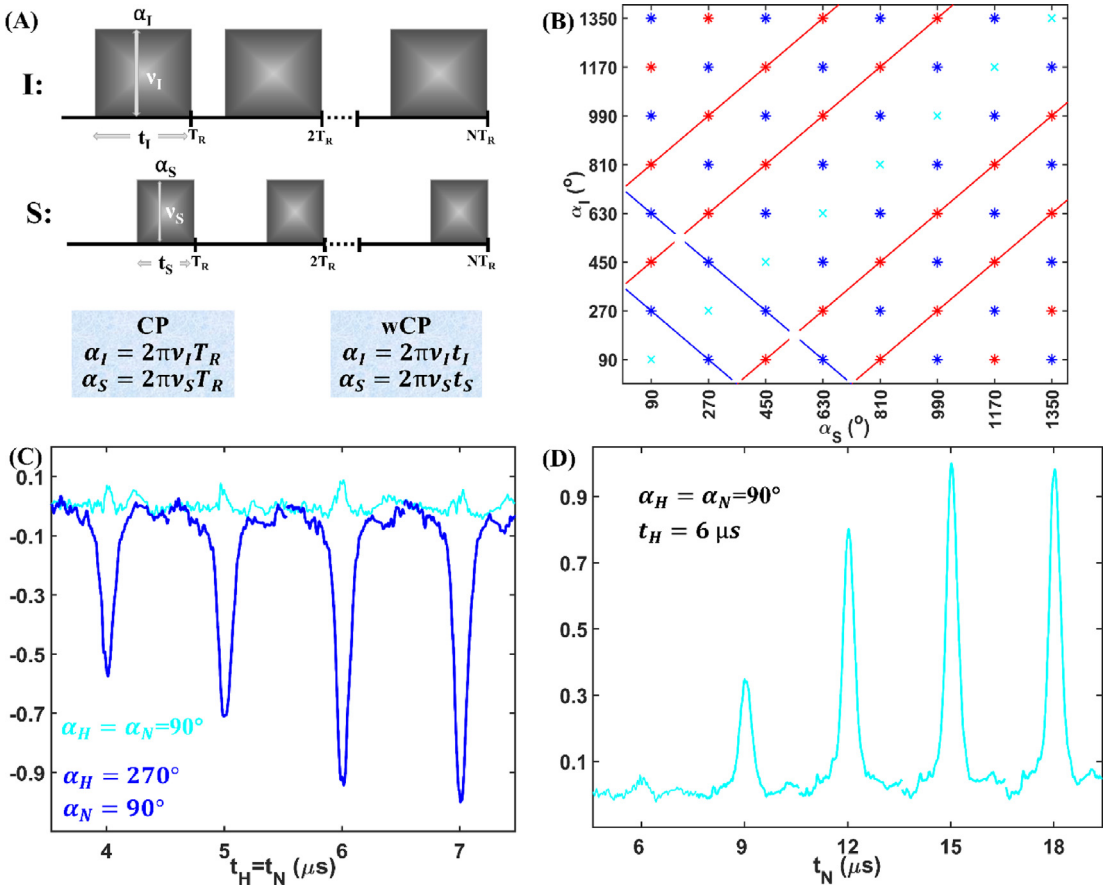


**Fig. 1.** (A) wCP. Each rotor period contains a single pulse on each channel with flip angles, lengths and rf-field strengths ($\alpha_I, t_I, \nu_I$) and ($\alpha_S, t_S, \nu_S$) on channels I and S, respectively. (B) Flip angle values for which the FOH was calculated (Eqns. (1 and 2). Red and blue stars represent positive and negative conditions. Red and blue lines represent the flip angles for CP (the pulse length is one rotor period on both channels), and the sum or difference between rf-field values match Hartmann-Hahn conditions [1]. The diagonal (cyan crosses) represents a special case, where positive transfer is observed if $t_I \neq t_S$. (C) and (D) wCP 1D (HN)H spectra as a function of windowed pulse parameters on proton and nitrogen channels. (C) with the condition $t_H = t_N$ and (D) as a function of windowed pulses on the nitrogen channel, $t_N$. In both panels, the $^1$H→$^{15}$N transfer was kept constant: CP with linear amplitude modulation 80 % →100 % of 102 kHz and 44 kHz on $^1$H and $^{15}$N channels, respectively, and 800 µs mixing. wCP was applied for $^{15}$N→$^1$H transfers. To calculate the power levels of pulses in watts, the reference values of 90° optimized pulses with lengths of 2.25 µs (111.111 kHz, proton channel) and 3.12 µs (80.128 kHz, nitrogen channel) were used. (C) 10 wCP $^{15}$N→$^1$H rotor periods ($t_{mix}$ = 180 µs) and $t_H = t_N$. Cyan spectra - $\alpha_H = \alpha_N = 90^\circ$. Blue spectra – $\alpha_H = 270^\circ$ and $\alpha_N = 90^\circ$. (D) 14 wCP $^{15}$N→$^1$H rotor periods ($t_{mix}$ = 252 µs) and $t_H = 6\mu s$. $t_N$ is varied from 6 to 18 µs. The data were acquired at a 600 MHz spectrometer with 55.555 kHz MAS and the M2 sample. (For interpretation of the references to colour in this figure legend, the reader is referred to the web version of this article.)

et al. in 2015 [58]. In the Supplementary Information (SI), two approximate solutions are derived. The first, Eq. S16, can qualitatively describe CP and wCP profiles with the same pulse lengths and an arbitrary set of flip angles applied on the two channels. (By wCP profile, we mean the transfer efficiency with respect to two rf-field strengths or flip angles). The second, Eq. S39, can qualitatively describe wCP profiles with different pulse lengths and flip angles. Figure S1 compares the approximate theoretical and numerically exact curves. Here we show the key points for the first approximate solution.

The transferred signal for wCP with a fictitious spin-1/2 formalism [74] and in the tilted rf-field frame [78] can be described as follows:

$$\langle S_x\rangle(t_{mix}) = \frac{1}{4}\int d\Omega\left[Tr\left\{\left(U_{tot}^{(1,4)}\right)^2\right\} - Tr\left\{\left(U_{tot}^{(2,3)}\right)^2\right\}\right], \quad (2)$$

where the integration over orientation ($\Omega$) indicates the usual averaging over powder Euler angles, $(\alpha, \beta, \gamma)$ [78]. $U_{tot}^{(1,4)}$ and $U_{tot}^{(2,3)}$ are DQ and ZQ unitary propagators. The derivation of the Eq. (2) is shown in the SI (Eq. (S1-S12)).

The first order ZQ and DQ Average Hamiltonian [79] (FOH) can be calculated for the following ZQ flip angle (FLAN) conditions, where $\alpha$ is the flip angle acquired by the spin I or S during one rotor period:

$$\Sigma_{IS} = \alpha_I + \alpha_S = \pi + 2\pi n \text{ and } \Delta_{IS} = \alpha_I - \alpha_S = 2\pi + 2\pi n', \quad n \geq n', \quad (3)$$

Then ZQ and DQ FOH are:

$$t_{mix}\tilde{H}_{ZQ}^{(1)} = N\left[\Phi_{Dx,\Sigma}I_x^{(2,3)} + \Phi_{Dy,\Sigma}I_y^{(2,3)}\right] \text{ and } t_{mix}\tilde{H}_{DQ}^{(1)} = 0. \quad (4)$$

On the other hand, with the following DQ FLAN conditions:

$$\Sigma_{IS} = \alpha_I + \alpha_S = 2\pi + 2\pi n \text{ and } \Delta_{IS} = \alpha_I - \alpha_S = \pi + 2\pi n', \; n \geq n', \quad (5)$$

ZQ and DQ FOH are:

$$t_{mix}\tilde{H}_{ZQ}^{(1)} = 0 \text{ and } t_{mix}\tilde{H}_{DQ}^{(1)} = \frac{1}{2T_R}\left[2\Phi_{Dx,\Delta}I_x^{(1,4)} + 2\Phi_{Dy,\Delta}I_y^{(1,4)}\right]. \quad (6)$$

$\Phi_{Dx,\Sigma \text{ or } \Delta}$ are the time integrated functions, which depend on the sums (for DQ) or the differences (for ZQ) between rf-field strength values and dipolar time dependent functions [78,80]. Their explicit forms are shown in the SI. For both cases the measured ZQ (positive, $\Delta$) and DQ (negative, $\Sigma$) signals are described with the next simple Eqn.:

$$S_x(t_{mix} = NT_R) \approx \pm 0.5 \times \int d\Omega\left[1 - cos\left(0.5N\sqrt{\left(\Phi_{Dx,\Sigma \text{ or } \Delta}\right)^2 + \left(\Phi_{Dy,\Sigma \text{ or } \Delta}\right)^2}\right)\right]. \quad (7)$$

The equation governing the signal transferred via wCP (Eq. (7)) has the same structure as for CP reported previously by Zhou and Ye [81]: the signal is composed of ZQ and DQ contributions with opposite signs. Such identity in the structure shows the connection between the CP and wCP sequences.

The schematic presentation of FLAN conditions for positive (red) and negative (blue) polarization transfers are shown in Fig. 1B. Red and blue stars show FLAN conditions for wCP, while red and blue lines show the set of flip angles for CP (the pulse length is one rotor period) Hartmann-Hahn conditions. Note the additional transfer conditions that appear for wCP. We note here a similarity to the related sequence, delays alternating with nutation for tailored excitation (DANTE). [82–83] The nutation behavior of the windowed pulses (for spins within the excitation bands of DANTE) during one rotor period can be approximated with the average nutation frequency over this period.

Along the diagonal of the wCP profile (Fig. 1B), the cyan crosses represent a special case where signal transfer occurs away from Hartmann Hahn conditions, but unlike other conditions, transfer is only observed if the pulse lengths applied on the two channels differ. In other words, for wCP if $\alpha_I = \alpha_S$ and $t_I = t_S$ the transferred signal is zero. This can be explained by the fact that under these conditions the rf-field Hamiltonian with a fictitious spin-1/2 formalism [74] only depends on DQ operators. Then the total ZQ Hamiltonian only depends on dipolar interaction, which results in $U_{tot}^{(2,3)} = 1$. The modified Eq. (2) can be written as:

$$\langle S_x\rangle(t_{mix}) = \int d\Omega\left[\frac{1}{4}Tr\left\{\left(U_{tot}^{(1,4)}\right)^2\right\} - \frac{1}{2}\right]. \quad (8)$$

$U_{tot}^{(1,4)}$ is calculated in the same way as before (Eqns. S8-S15 in SI). If we apply the diagonal flip angle conditions:

$$\alpha_I = \alpha_S = \frac{\pi}{2} + \pi n, \quad (9)$$

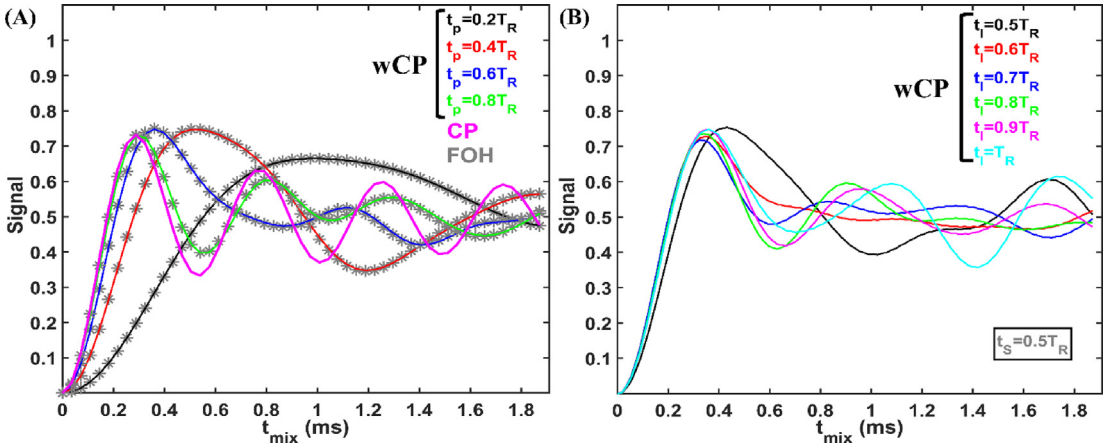


**Fig. 2.** wCP curves. For both (A) and (B) the MAS was 55.555 kHz (18 μs rotor period) and the spin system was two spins with 6 kHz dipolar coupling. The same flip angle set, ($\alpha_I = 630^\circ$, $\alpha_S = 270^\circ$), was applied. (A) First Order Average Hamiltonian Approximation (gray stars) and numerical simulation (solid lines) as a function of mixing time under different pulse lengths (equal lengths on each channel, $t_I = t_S = t_p$). The pink solid line represents CP experiments that satisfy the Hartmann-Hahn condition. (B) Numerical simulations, where the pulse length on *S* channel was the same ($t_S = 0.5T_R$) and the pulse length on the *I* channel was varied as labeled in the legend. (For interpretation of the references to colour in this figure legend, the reader is referred to the web version of this article.)

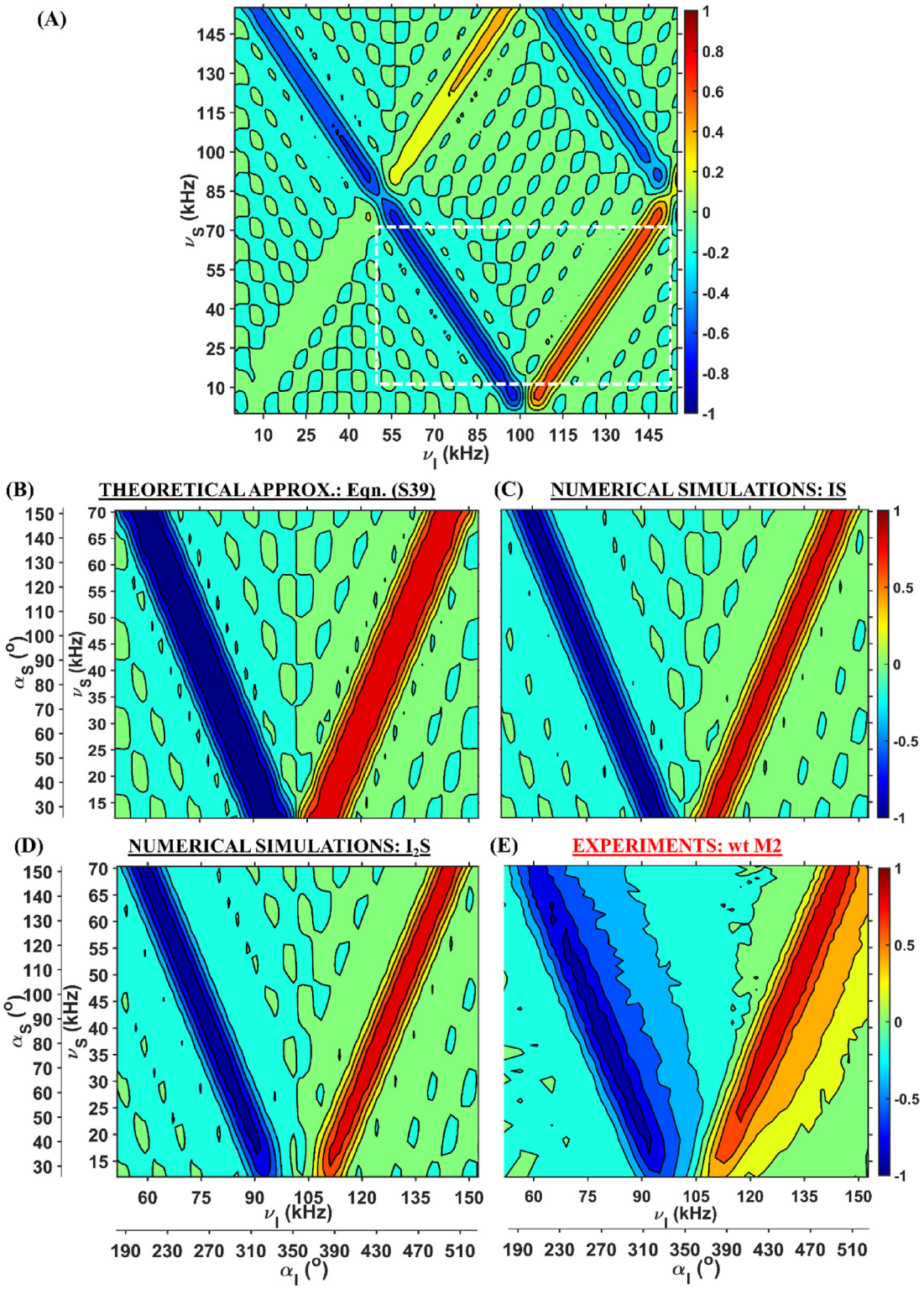


**Fig. 3.** wCP profiles: the transferred signal intensity ($t_{mix}$ = 0.18 ms) as a function of applied rf-field, obtained with windowed pulses. (A) Broad numerical profile. The dashed rectangle indicates the experimentally investigated area, which was investigated theoretically, numerically and experimentally (B-E). Theoretical approximate (B), numerical (C-D) and experimental (E) profiles. On $^1$H (I spin) and $^{15}$N (S spin) the lengths of the applied pulses were 9.8 and 6 μs, respectively (windows of 8.2 μs and 12 μs). (B) The theoretical approximate wCP profile was obtained with Eq. S39 (see the SI). (A, C) The numerical simulation considered an *IS* spin system with heteronuclear dipolar couplings of 11 kHz. (D) The numerical simulation considered an $I_2S$ spin system with heteronuclear dipolar couplings of 11 kHz and 3.2 kHz and a homonuclear dipolar coupling of 5 kHz. (E) Experimental data were recorded in 1D following (HN)H transfer, with polarization transfer conditions from $^1$H to $^{15}$N kept constant (ramp CP with 0.72 ms mixing) and the polarization transfer conditions for $^{15}$N to $^1$H CP varied. Data were acquired at a 600 MHz spectrometer with 55.555 kHz MAS using a sample of M2. Full experimental details are given in the SI.

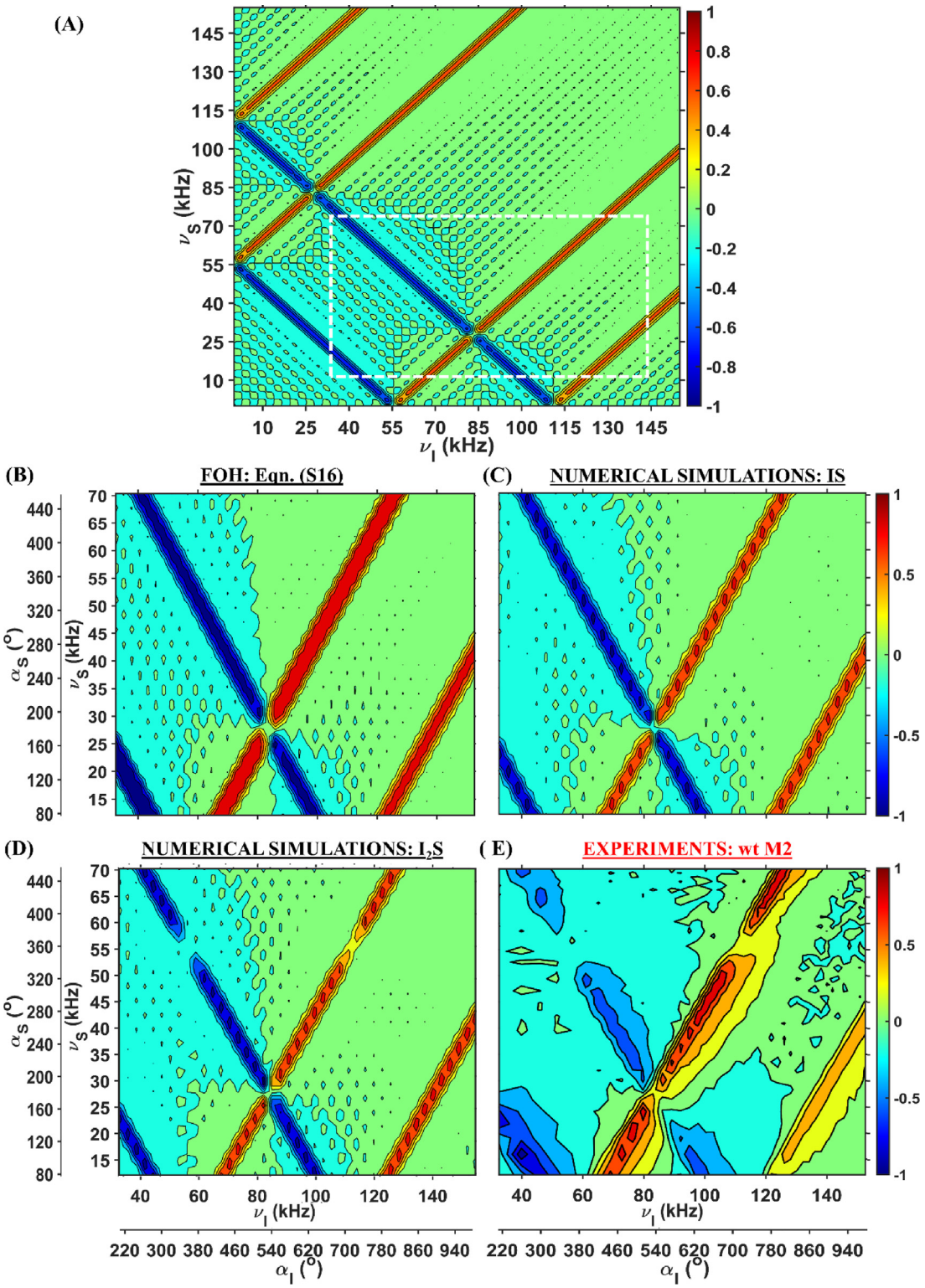


**Fig. 4.** CP profiles: the transferred signal intensity ($t_{mix}$ = 0.18 ms) as a function of applied rf-field. Broad numerical profile (A), first order Hamiltonian (B), numerical (C-D) and experimental (E) transferred signal intensity ($t_{mix}$ = 0.18 ms) as a function of applied rf-field, obtained with continuous pulses. The dashed rectangle indicates the experimentally investigated area, which was investigated theoretically, numerically and experimentally (B-E). (B) Analytical CP profile was obtained with first order approximation of the Hamiltonian (Eq. S16). (A, C) The CP simulations considered an *IS* spin system with heteronuclear dipolar couplings of 11 kHz. (D) The CP simulations considered an $I_2S$ spin system with heteronuclear dipolar couplings of 11 kHz and 3.2 kHz and a homonuclear dipolar coupling of 5 kHz. (E) Experimental data were recorded in 1D following (HN)H transfer, with polarization transfer conditions from $^1$H to $^{15}$N kept constant (ramp CP with 0.72 ms mixing) and the polarization transfer condition for $^{15}$N to $^1$H CP varied. Data were acquired at a 600 MHz spectrometer with 55.555 kHz MAS using a sample of M2. Full experimental details are given in the SI.

then at points $N \in$ even, the DQ FOH is:

$$t_{mix}\tilde{H}^{(1)}_{DQ} = 0, \tag{10}$$

and:

$$U^{(1,4)}_{tot} \approx 1. \tag{11}$$

Substituting Eq. (12) into Eq. (9), we obtain that the measured signal is zero:

$$\langle S_x(t_{mix} = NT_R)\rangle \approx 0 \tag{12}$$

In summary, wCP results in transfer along the diagonal of the profile ($\alpha_I = \alpha_S$) when $t_I \neq t_S$.

Fig. 1C and D confirm this conclusion, where we show the experimental wCP 1D (HN)H spectra as a function of pulse lengths and flip angle values.

When we keep $\alpha_H = \alpha_N = 90^\circ$ and $t_H = t_N$ (cyan spectra in Fig. 1C), we observe a noise level signal. By contrast, for the condition $\alpha_H = 270^\circ$, $\alpha_N = 90^\circ$ and $t_H = t_N$, negative DQ transfer is observed (blue spectra in Fig. 1C).

Fig. 1D shows the dependence of the pulse length difference: $\alpha_H = \alpha_N = 90^\circ$ and $t_N \geq t_H$. With increasing difference between $t_N$

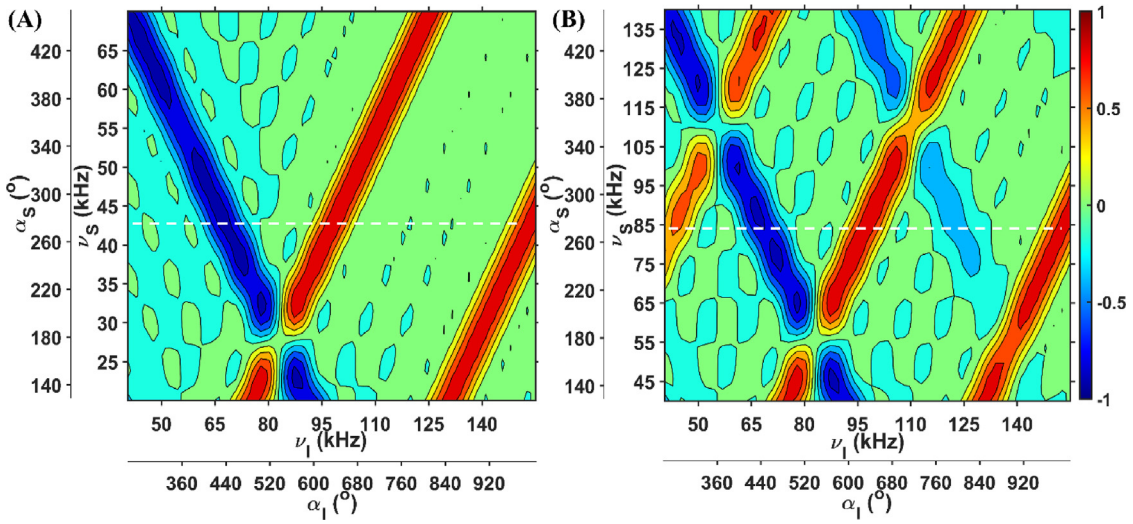


**Fig. 5.** Simulation of CP (A) and wCP (B). For both cases, the numerical simulations considered an $I_2S$ spin system with heteronuclear dipolar couplings, 21 kHz and 7.2 kHz and a homonuclear dipolar coupling of 8 kHz. The mixing time is 90 µs and the MAS rate 55.555 kHz. (A) Continuous pulses on *I* and *S* spins. (B) Continuous pulses on *I* spins and windowed pulse every rotor period with 9 µs length on the *S* spin. The dashed white lines show the slices that were experimentally recorded and shown in Fig. 6.

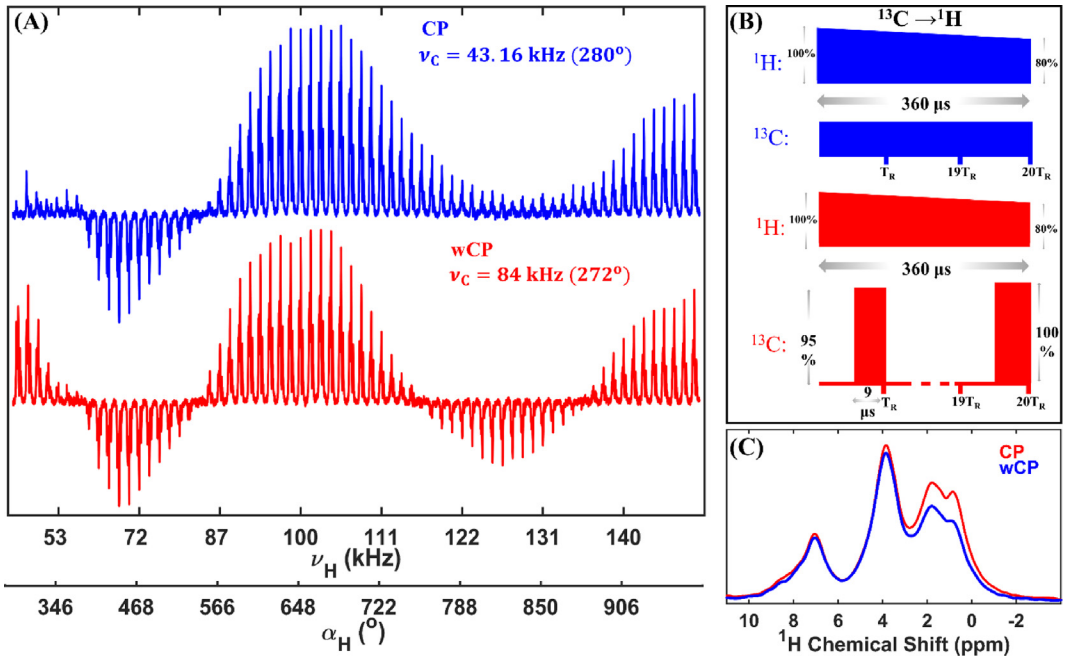


**Fig. 6.** (A) CP (blue) and wCP (red) 1D (HC)H CP spectra as a function of $^{1}H$ rf-field strength with different $^{13}C$ pulse lengths / rf-field strengths: blue - continuous / 43.16 kHz and red 9 µs / 84 kHz. (B) Schematic presentation of the pulse sequence for $^{13}C \rightarrow ^{1}H$ transfer, with continuous (blue) and windowed (red) pulses on the $^{13}C$ channel. Linear ramped amplitude modulation, 100%→80%, was applied on the $^{1}H$ channel. In both cases, the $^{1}H \rightarrow ^{13}C$ transfer was kept constant, while $^{13}C \rightarrow ^{1}H$ conditions were varied. The carrier frequency was set to 100 ppm. The mixing time for both transfers was 360 µs. Figure C compares 1D CP (red) and wCP (blue) (HC)H spectra with the best performance for each case. The data were acquired at a 600 MHz spectrometer with 55.555 kHz MAS and the M2 sample. Additional experimental details are given in the SI. (For interpretation of the references to colour in this figure legend, the reader is referred to the web version of this article.)

and $t_H$, the positive signal (ZQ dominating) increases. Note that the signal in panels C and D are not to scale, and that the signal along the diagonal of the profile is typically not the most efficient (*vide infra*).

We next focus on conditions where $\alpha_I \neq \alpha_S$.

In Fig. 2 we compare the numerical and FOH (Eq. (7)) curves. Fig. 2A shows the comparison of the numerical (solid lines) and analytical (gray stars) curves as a function of mixing time for different pulse lengths on both channels (keeping $t_I = t_S = t_p$). We observe a good agreement between numerical and FOH curves. While the size of the window has an influence on the effective dipolar scaling factor, for some pulse lengths the theoretical efficiency of wCP reaches 75%.

Fig. 2B shows numerical curves with the pulse length on one channel kept constant ($t_S$ = 0.5$T_R$) and the pulse length of the second channel varied from 0.5$T_R$ to $T_R$ (no window). In this case, we also observe similar transfer efficiencies, but with equal pulse lengths on both channels wCP achieves a slightly better performance.

While in numerical simulation, the rf-field strength is not restricted, for experiments high power cannot be reached for low gamma spins. We therefore limited our experimental profiles to the areas indicated with dashed rectangles in Fig. 3A for wCP and Fig. 4A for CP. Fig. 3B-E and 4B-E compare the theoretical (B), numerical (C-D) and experimental (E) wCP (Fig. 3) and CP (Fig. 4) profiles. For Figs. 3 and 4 we observe a good agreement between theoretical (B) and two spin system simulated (C) profiles, as well as three spin system simulation (D) and experimental (E) profiles.

Fig. 3 shows that over a broad range of flip angle values, wCP provides polarization transfers and the main effect depends on the sums or differences between flip angles. Note that since the sequence is rotor synchronized, the dependence on flip angle could equally be described as a dependence on the average rf-field strength (average nutation frequency).

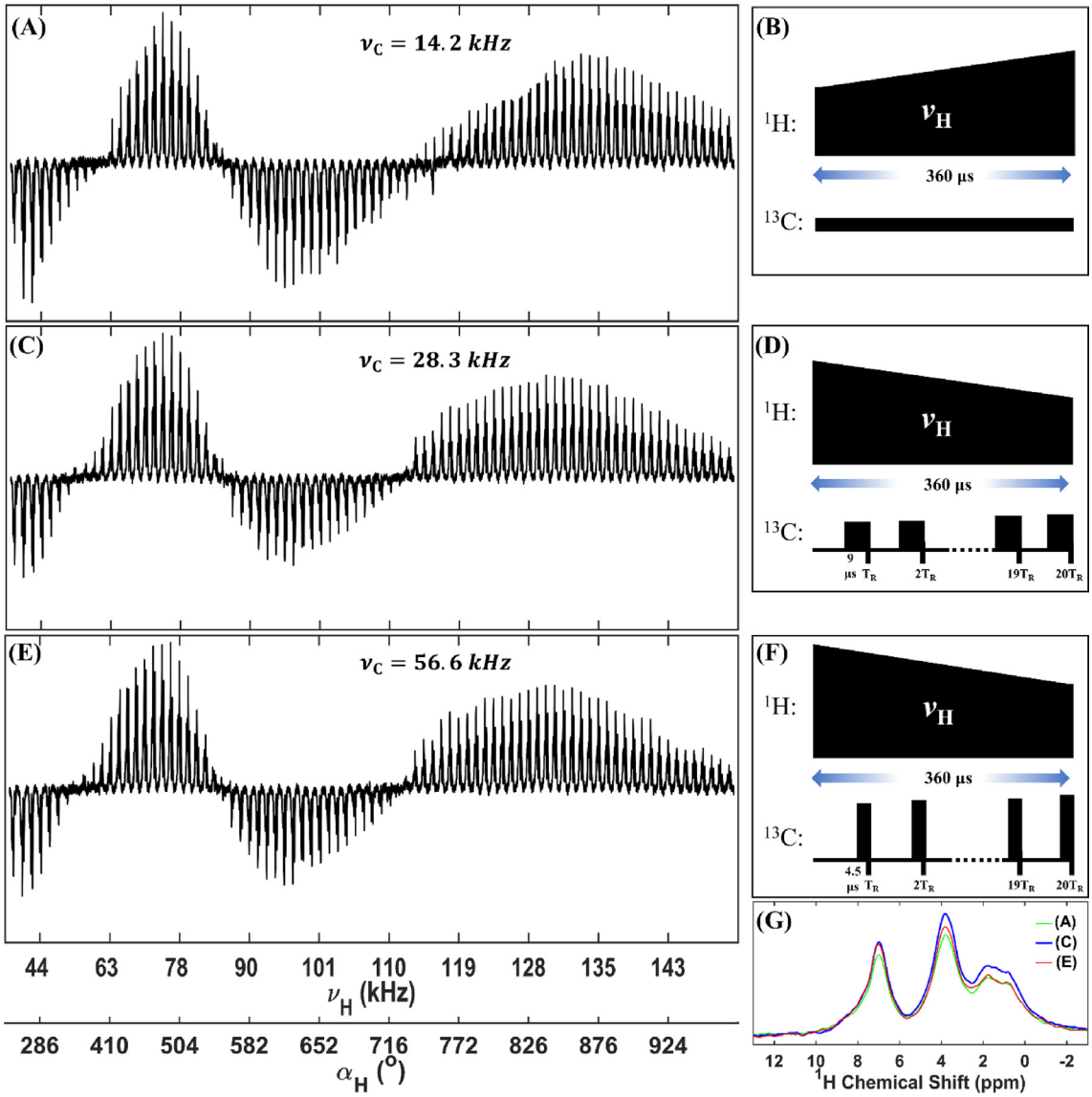


**Fig. 7.** CP (A) and wCP (C, E) 1D (HC)H spectra as a function of $^1$H rf-field strength (for $^1$H→$^{13}$C transfer) with different $^{13}$C rf-field strengths and pulse lengths: (A) CP: 14.2 kHz; (C) wCP: 28.3 kHz and 9 µs and (E) wCP: 56.6 kHz and 4.5 µs. Figure F compares 1D CP and wCP (HC)H spectra with the best performance for each case. (B), (D) and (F) depict the $^1$H→$^{13}$C cross polarization pulse sequence, which was used in each case. The ramped $^{13}$C→$^1$H cross polarization step was kept the same with an optimized ZQ Hartmann-Hahn condition. The spectra were acquired at a 600 MHz spectrometer with 55.555 kHz MAS and the M2 sample. The carrier frequency was set to 135 ppm. Further experimental details are given in the SI.

For Fig. 4 there is a difference between three spin system (D) and two spin system (C) simulations. In these two figures we observe additional gaps, which are not seen in two-spin system simulations (Fig. 4C). These gaps are related to homonuclear rotary resonance recoupling at about 55 and 110 kHz for the *I* spin.

While Fig. 3E and Fig. 4E demonstrate wCP and CP profiles at a specific mixing time, Fig. S2A shows the comparison of the experimental CP and wCP curves as a function of the mixing times. Similar build up curves are observed for both cases.

The ratio between rf-field strength values (in kHz) of CP and wCP sequences has an inverse dependence on the normalized pulse length: $(t_p/T_R)^{-1}$. However, the requirement of the rf-field power values in Watts for windowed pulses is squared in comparison to the ratio in kHz, leading to a ratio for rf-field power values of $(t_p/T_R)^{-2}$. Therefore, the application of this sequence might be limited at ultra-fast MAS rates, especially for ZQ transfers. On the other hand, faster MAS rates are typically achieved through the use of a smaller rotor and coil, leading to an improvement in the maximum possible rf-field strength. A low power condition also exists in the wCP sequence (*vide infra*) with matching flip angles on the two channels. It is not particularly efficient under the conditions reported here, but might be interesting for future developments, e.g. > 200 kHz MAS where the required rf-field strength for CP becomes extreme.

In Figs. 3 and 4 we kept similar rf-field strength ranges. In this case, CP and wCP profiles appear to be different. However, according to the derivations in the SI, if we rescale according to the flip angle, CP and wCP profiles should share common features. This is demonstrated in Fig. 5. For wCP (Fig. 5B) the windowed pulses were applied on the S spin only and continuous rf-field power was applied on the I spin.

With CP (Fig. 5A) we observe the expected one DQ and two ZQ conditions within this region, according to the Hartmann Hahn conditions [1]. Comparing CP (A) and wCP (B) profiles we obtain a full match for these one DQ and two ZQ conditions in the flip angle domain. However, an additional positive transfer and an additional negative transfer are observed for wCP.

For wCP the additional positive transfer (red) is observed when equal flip angle values are applied on both channels, e. g. at $\alpha_I = \alpha_S = 270^\circ$. As was explained above (and demonstrated experimentally with Fig. 1D) such transfers are only observed when the pulse lengths on the two channels differ. The additional negative transfer (blue) is observed with the next flip angle set, $\alpha_I = 810^\circ$, $\alpha_S = 270^\circ$, according to FLAN conditions (Fig. 1B).

To experimentally demonstrate the matching conditions visible in Fig. 5, two slices from the CP and wCP profiles were recorded (the dashed white lines of Fig. 5). The experimental data is shown in Fig. 6, where the upper spectra were recorded with CP (blue) and the lower with wCP (red). As in simulation, we observe three transfer conditions for CP, and 5 for wCP.

One of the additional transfer conditions for wCP is observed in Fig. 6 when the applied pulses on different channels have the same flip angles. This transfer condition is an additional example of the those seen along the cyan diagonal in Fig. 1A. Note that second order CP [84–85] also lies along the diagonal, but is typically less efficient than ZQ or DQ CP.

Fig. 6C compares CP (red) and wCP (blue) (HC)H spectra with the highest performance from each profile. In that case we observe better performance for CP, especially in the methyl region. However, note that the relatively short transfer time might not be optimal for wCP, given the reduced scaling factor as compared with CP (Fig. 1 and Fig. S2A).

To improve performance despite rf-field inhomogeneity, a small ramped amplitude modulation (from 95% to 100%) can be additionally applied on the second channel for windowed pulses. Similar to ramped CP [41] a linear ramped amplitude improves the performance. The benefit of amplitude modulation was also demonstrated in $^{\text{RESPIRATION}}$CP experiments [86]. Although we mostly found that the amplitude modulation on one of the channels was enough to reduce the influences of rf-field inhomogeneity and offset, in some cases we applied an additional small ramped amplitude modulation on the second channel to further improve the performance. Fig. S3 demonstrates such a case, comparing 1D (HC)H spectra with amplitude modulation on both channels.

The previous comparison of CP and wCP was made using strong rf-field strengths, applied on both channels. Under these conditions we did not find any clear advantage of using wCP with respect to CP. In contrast, we found that wCP can outperform CP when low rf-field strength (small flip angle) is applied on at least one of the channels. Baldus et al. [44] in 1998 and Laage et al. [87] in 2008 demonstrated that low rf-field strength applied on

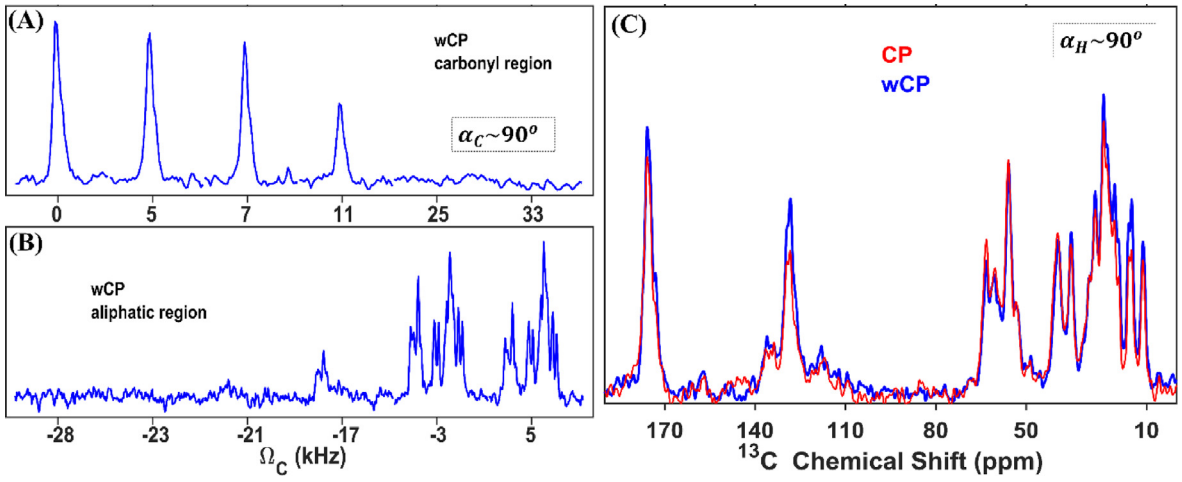


**Fig. 8.** (A)-(B) Experimental 1D wCP (H)C spectra as a function of offset with respect to carbonyl (A, 175 ppm is on resonance) and aliphatic regions (B, 35 ppm is on resonance). The $^{1}$H channel conditions were 15 µs / 78.38 kHz pulses and linear ramp (100%→90%) and the $^{13}$C channel conditions were 6 µs / 44.6 kHz pulses with linear ramp (95%→100%). In all cases 540 µs contact time was used. (C) Experimental 1D CP (red) and wCP (blue) (H)C spectra with the same flip angle sets ($\alpha_H$ 90°): for CP 67 kHz and 19 kHz (80%→100%, linear ramp) were applied on $^{13}$C and $^{1}$H channels, respectively, while for wCP 64 kHz (no windows, 95%→100% linear ramp) and 57 kHz (6 µs pulses with 80%→100% linear ramp) were applied on $^{13}$C and $^{1}$H channels, respectively. 360 µs contact time was used. The data were acquired at an 800 MHz spectrometer with 55.555 kHz MAS and using S31N M2. Additional experimental details are given in the SI. (For interpretation of the references to colour in this figure legend, the reader is referred to the web version of this article.)

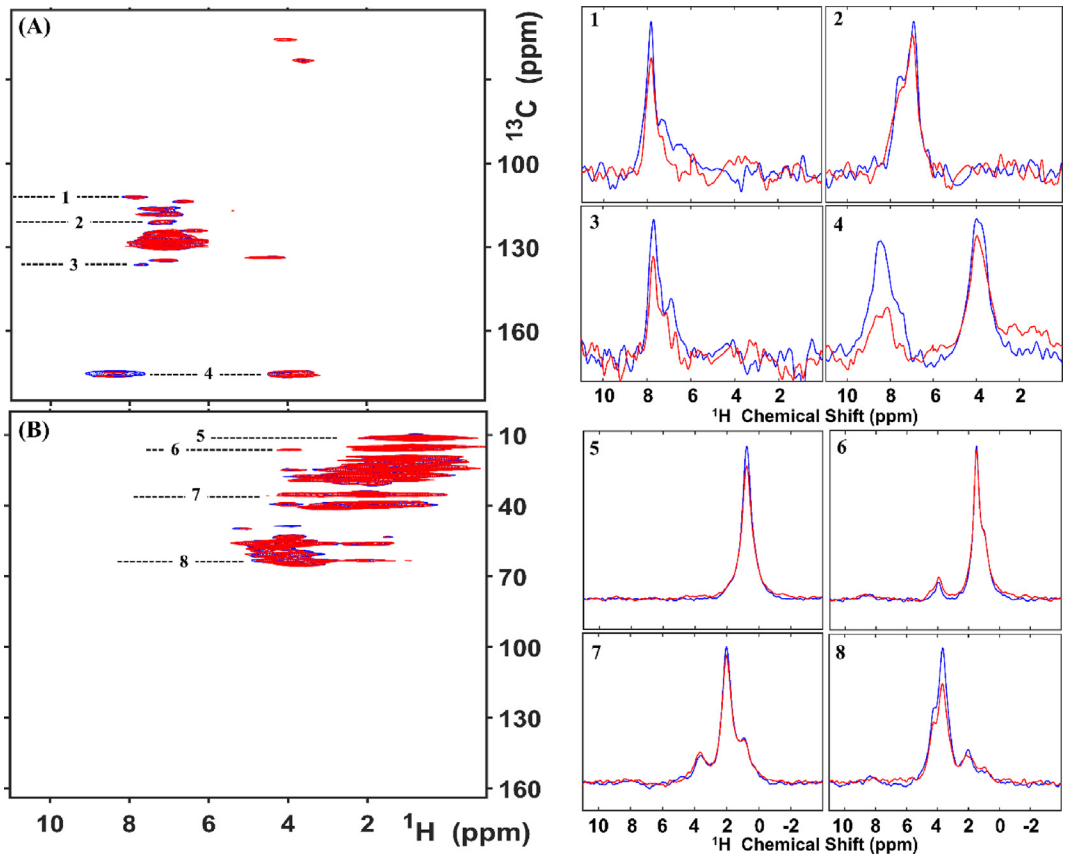


**Fig. 9.** SPECIFIC-CP (red) and SPECIFIC-wCP (blue) 2D (H)CH spectra. (A) The carrier frequency position was set to 135 ppm. (B) The carrier frequency position was set to 25 ppm. The data were acquired at an 800 MHz spectrometer with 55.555 kHz MAS and using S31N M2. The full experimental details are given in the SI. The slices from 2D experiments are indicated with numbers 1–8. (For interpretation of the references to colour in this figure legend, the reader is referred to the web version of this article.)

the $^{13}$C channel allowed transfer to select regions of the spectrum. The method was named SPECIFIC-CP. Such conditions result in a $^{13}$C flip angle of around 90° for the SPECIFIC-CP conditions. The application of wCP with about 90° pulses on $^{13}$C channel also preserves the band-selectivity despite the higher rf-field strength. This is demonstrated in Figs. 7-9.

Fig. 7 shows 1D (HC)H spectra as a function of $^{1}$H flip angle (and rf-field strength) for CP and wCP while maintaining a 90° flip angle on the $^{13}$C channel. The shape of the profile is maintained. The pulse lengths on the $^{13}$C channel are 18 μs (A, CP), 9 μs (C, wCP) and 4.5 μs (E, wCP). For wCP higher rf-field strengths are applied to achieve the same flip angle value as for CP. The rf-field strength of these pulses on the $^{13}$C channel required to maintain a 90° flip angle were then: 14.2 kHz (A), 28.3 kHz (C) and 56.6 kHz (E). With respect to rf-field power levels in Watts (W) these values were: 0.85 W, 3.42 W and 13.6 W, respectively. Fig. 7F compares CP (green) and wCP (blue, red) (HC)H spectra with the highest performance from each profile. Note that there appears to be an improvement in ZQ polarization transfer for wCP (positive signals) and a decrease in performance for DQ polarization transfer. Fig. S4 demonstrates similar experiments, acquired at an 800 MHz spectrometer.

We next take a closer look at the band-selectivity with application of 90° pulses on the $^{13}$C channel in wCP experiments. Fig. 8A-B demonstrates the dependence of carbonyl (A) and aliphatic (B) regions on offset values with 44.6 kHz rf-field strength on the $^{13}$C channel. As can be seen, beyond a 23 kHz offset the carboxyl (A) and aliphatic (B) region are not observed. Despite high rf-field strength, the band-selectivity is preserved. Similar to SPECIFIC-CP, the application of windowed 90° pulses on the $^{13}$C channel can be called a SPECIFIC-wCP.

When in reverse 90° pulses are applied on the $^{1}$H channel (Fig. 8C), more complete band excitation is observed: all regions of the $^{13}$C spectrum have similar intensities. Under these conditions, 67 kHz is applied on the $^{13}$C channel for the CP case, and the flip angle is 450° for both CP and wCP. The carrier frequency was set to 100 ppm. The comparison of CP (red) and wCP (blue) spectra shows better performance for wCP under these conditions.

The higher performance for SPECIFIC-wCP with respect to SPECIFIC-CP can be more clearly observed from 2D (H)CH experiments (Fig. 9), where the carrier frequency is set to the aromatic region (135 ppm, A) or aliphatic region (B, 25 ppm). Selected slices from these data are shown at the right. For all regions, SPECIFIC-wCP has an improved performance as compared with SPECIFIC-CP. In particular, in slice 4, a twofold improvement is observed for carbonyl to amide proton transfer. In general, a larger improvement is seen towards the edges of the specific band.

In the SI we show 2D wCP (H)CH spectra acquired at a 1200 MHz spectrometer, where ~ 90° pulses were applied on the $^{1}$H channel (Figure S5). Also in that case we observe more complete excitation of the $^{13}$C region. CP and wCP profiles for weak dipolar coupling pairs (e.g. $^{13}$C-$^{15}$N) are compared in Figure S6.

## 3. Conclusions

Cross polarization transfers between heteronuclear spins is a fundamental building block used in MAS NMR, where the transfers via dipolar interactions are usually explained with Hartmann-Hahn conditions [1]. These conditions declare that maximal transfer occurs when the difference or the sum between applied spin-lock rf-field strengths is an integer, n, times the MAS rate (n=±1,±2).

In this article we theoretically investigated windowed CP sequences (wCP) that had a single window per rotor period, and derived the flip angle conditions (FLAN), under which zero-quantum and double-quantum transfers were observed. A theoretical approximation of the transfer, as well as numerically exact simulations of two to three spins, were in good agreement with experimental CP and wCP profiles. We showed that the CP and wCP transfer conditions can be best compared with respect to the rf pulse flip angles, or equivalently, the average spin-lock rf-field strengths. This revealed a close connection between wCP and CP, namely that the wCP sequence shares conditions of efficient transfer with CP, and also has additional transfer conditions of lower efficiency. Given the similarity between the two sequences, it is perhaps unsurprising that they performed equally well most of the time (note we only considered fast MAS conditions where windows do not cause problems with spin locking). Nevertheless, a benefit in transfer efficiency was observed for wCP for a SPECIFIC-CP transfer condition with small $^{13}C$ flip angle. Surprisingly, the higher rf-field strength on $^{13}C$ for wCP experiments did not eliminate the band-selectivity. The wCP sequence also showed an improvement in transfer efficiency with 90° pulses on the $^{1}H$ channel and 450° pulses on the $^{13}C$ channel, conditions under which the transfer has a broad bandwidth.

## 4. Experimental methods

The full experimental details are given in the SI.

## Data availability

Data will be made available on request.

## Declaration of Competing Interest

The authors declare that they have no known competing financial interests or personal relationships that could have appeared to influence the work reported in this paper.

## Acknowledgments

We acknowledge financial support from the MPI for Multidisciplinary Sciences, and from the Deutsche Forschungsgemeinschaft (Emmy Noether program Grant AN1316/1-1). We thank Melanie Wegstroth and Kerstin Overkamp for synthesis and purification of M2 samples. We thank Dr. Dirk Bockelmann and Brigitta Angerstein for technical assistance.

## Appendix A. Supplementary material

Supplementary data to this article can be found online at https://doi.org/10.1016/j.jmr.2023.107404.

## References

[1] M. Emshwiller, E.L. Hahn, D. Kaplan, Pulsed Nuclear Resonance Spectroscopy, Phys. Rev. 118 (1960) 414–424.
[2] J. Schaefer, E.O. Stejskal, Carbon-13 nuclear magnetic resonance of polymers spinning at the magic angle, J. Am. Chem. Soc. 98 (1976) 1031–1032.
[3] P.-H. Chien, K.J. Griffith, H. Liu, Z. Gan, Y.-Y. Hu, Recent advances in solid-state nuclear magnetic resonance techniques for materials research, Annu. Rev. Mater. Res. 50 (2020) 493–520.
[4] A. Brinkmann, M.H. Levitt, Symmetry principles in the nuclear magnetic resonance of spinning solids: heteronuclear recoupling by generalized Hartmann-Hahn sequences, J. Chem. Phys. 115 (2001) 357–384.
[5] T. Gullion, J. Schaefer, Rotational-echo double-resonance NMR, J. Magn. Reson. 1969 (81) (1989) 196–200.
[6] A.W. Hing, S. Vega, J. Schaefer, Transferred-echo double-resonance NMR, J. Magn. Reson. 1969 (96) (1992) 205–209.
[7] E.R.H. van Eck, R. Janssen, W.E.J.R. Maas, W.S. Veeman, A novel application of nuclear spin-echo double-resonance to aluminophosphates and aluminosilicates, Chem. Phys. Lett. 174 (1990) 428–432.
[8] T. Gullion, A.J. Vega, Measuring heteronuclear dipolar couplings for I=1/2, S>1/2 spin pairs by REDOR and REAPDOR NMR, Prog. Nucl. Magn. Reson. Spectrosc. 47 (2005) 123–136.
[9] Z. Gan, Measuring multiple carbon– nitrogen distances in natural abundant solids using R-RESPDOR NMR, Chem. Commun. (2006) 4712–4714.
[10] L. Chen et al., Measurement of hetero-nuclear distances using a symmetry-based pulse sequence in solid-state NMR, Phys. Chem. Chem. Phys. 12 (2010) 9395–9405.
[11] E. Nimerovsky, A. Goldbourt, Efficient rotational echo double resonance recoupling of a spin-1/2 and a quadrupolar spin at high spinning rates and weak irradiation fields, J. Magn. Reson. 206 (2010) 52–58.
[12] E. Nimerovsky et al., Phase-modulated LA-REDOR: A robust, accurate and efficient solid-state NMR technique for distance measurements between a spin-1/2 and a quadrupole spin, J. Magn. Reson. 244 (2014) 107–113.
[13] X.C. Zhang, M.C. Forster, E. Nimerovsky, K.T. Movellan, L.B. Andreas, Transferred-Rotational-Echo Double Resonance, J. Phys. Chem. A 125 (2021) 754–769.
[14] Y. Ji, L. Liang, X. Bao, G. Hou, Recent progress in dipolar recoupling techniques under fast MAS in solid-state NMR spectroscopy, Solid State Nucl. Magn. Reson. 112 (2021).
[15] G. Hou, I.-J.-L. Byeon, J. Ahn, A.M. Gronenborn, T. Polenova, 1H–13C/1H–15N heteronuclear dipolar recoupling by R-Symmetry sequences under fast magic angle spinning for dynamics analysis of biological and organic solids, J. Am. Chem. Soc. 133 (2011) 18646–18655.
[16] J. Struppe, C.M. Quinn, S. Sarkar, A.M. Gronenborn, T. Polenova, Ultrafast 1H MAS NMR crystallography for natural abundance pharmaceutical compounds, Mol. Pharm. 17 (2020) 674–682.
[17] Y. Nishiyama, Solid-State NMR Under Ultrafast MAS Rate of 40–120 kHz, in: *Experimental Approaches of NMR Spectroscopy: Methodology and Application to Life Science and Materials Science* (ed. The Nuclear Magnetic Resonance Society of Japan), Springer, 2018, pp. 171–195.
[18] S. Penzel et al., Spinning faster: protein NMR at MAS frequencies up to 126 kHz, J. Biomol. NMR 73 (2019) 19–29.
[19] K. Xue et al., Magic-Angle spinning frequencies beyond 300 kHz are necessary to yield maximum sensitivity in selectively methyl protonated protein samples in solid-state NMR, J. Phys. Chem. C 122 (2018) 16437–16442.
[20] B. Reif, R.G. Griffin, 1H detected 1H,15N correlation spectroscopy in rotating solids, J. Magn. Reson. 160 (2003) 78–83.
[21] D.H. Zhou et al., Solid-State Protein-Structure Determination with Proton-Detected Triple-Resonance 3D Magic-Angle-Spinning NMR Spectroscopy, Angew. Chem. Int. Ed. 46 (2007) 8380–8383.
[22] V. Chevelkov et al., H Detection in MAS solid-state NMR spectroscopy of biomacromolecules employing pulsed field gradients for residual solvent suppression, J. Am. Chem. Soc. 125 (2003) 7788–7789.
[23] D.H. Zhou et al., Proton-Detected Solid-State NMR Spectroscopy of Fully Protonated Proteins at 40 kHz Magic-Angle Spinning, J. Am. Chem. Soc. 129 (2007) 11791–11801.
[24] L.B. Andreas, T. Le Marchand, K. Jaudzems, G. Pintacuda, High-resolution proton-detected NMR of proteins at very fast MAS, J. Magn. Reson. 253 (2015) 36–49.
[25] L. Liang et al., Solid-State NMR dipolar and chemical shift anisotropy recoupling techniques for structural and dynamical studies in biological systems, Chem. Rev. 122 (2022) 9880–9942.
[26] S. Ahlawat, K.R. Mote, N.-A. Lakomek, V. Agarwal, Solid-State NMR: methods for biological solids, Chem. Rev. 122 (2022) 9643–9737.
[27] T. Le Marchand et al., 1H-Detected biomolecular NMR under fast magic-angle spinning, Chem. Rev. 122 (2022) 9943–10018.
[28] A.W. Overhauser, Polarization of nuclei in metals, Phys. Rev. 92 (1953) 411–415.
[29] T.R. Carver, C.P. Slichter, Polarization of nuclear spins in metals, Phys. Rev. 92 (1953) 212–213.
[30] Y. Su, L. Andreas, R.G. Griffin, Magic angle spinning NMR of proteins: high-frequency dynamic nuclear polarization and 1H detection, Annu. Rev. Biochem. 84 (2015) 465–497.
[31] T. Biedenbänder, V. Aladin, S. Saeidpour, B. Corzilius, Dynamic nuclear polarization for sensitivity enhancement in biomolecular solid-state NMR, Chem. Rev. 122 (2022) 9738–9794.
[32] A.J. Rossini et al., Dynamic nuclear polarization surface enhanced NMR spectroscopy, Acc. Chem. Res. 46 (2013) 1942–1951.
[33] D. Marks, S. Vega, A theory for cross-polarization NMR of nonspinning and spinning samples, J. Magn. Reson. A 118 (1996) 157–172.
[34] E.O. Stejskal, J. Schaefer, J.S. Waugh, Magic-angle spinning and polarization transfer in proton-enhanced NMR, J. Magn. Reson. 1969 (28) (1977) 105–112.
[35] D. Rovnyak, Tutorial on analytic theory for cross-polarization in solid state NMR, Concepts Magn. Reson. Part A 32A (2008) 254–276.
[36] J.-P. Amoureux, M. Pruski, Theoretical and experimental assessment of single- and multiple-quantum cross-polarization in solid state NMR, Mol. Phys. 100 (2002) 1595–1613.
[37] A.B. Nielsen et al., Simultaneous acquisition of PAR and PAIN spectra, J. Biomol. NMR 52 (2012) 283–288.
[38] B.B. Das, S.J. Opella, Simultaneous cross polarization to 13C and 15N with 1H detection at 60kHz MAS solid-state NMR, J. Magn. Reson. 262 (2016) 20–26.

[39] E.O. Stejskal, J. Schaefer, R.A. McKay, High-resolution, slow-spinning magic-angle carbon-13 NMR, J. Magn. Reson. 1969 (25) (1977) 569–573.
[40] O.B. Peersen, X.L. Wu, I. Kustanovich, S.O. Smith, Variable-amplitude cross-polarization MAS NMR, J. Magn. Reson. A 104 (1993) 334–339.
[41] G. Metz, X.L. Wu, S.O. Smith, Ramped-Amplitude cross polarization in magic-angle-spinning NMR, J. Magn. Reson. A 110 (1994) 219–227.
[42] S. Hediger, B.H. Meier, R.R. Ernst, Adiabatic passage Hartmann-Hahn cross polarization in NMR under magic angle sample spinning, Chem. Phys. Lett. 240 (1995) 449–456.
[43] S.V. Dvinskikh, V.I. Chizhik, Cross-polarization with radio-frequency field phase and amplitude modulation under magic-angle spinning conditions, J. Exp. Theor. Phys. 102 (2006) 91–101.
[44] M. Baldus, A.T. Petkova, J. Herzfeld, R.G. Griffin, Cross polarization in the tilted frame: assignment and spectral simplification in heteronuclear spin systems, Mol. Phys. 95 (1998) 1197–1207.
[45] T. Kamihara, K. Takegoshi, Rotational resonance for a heteronuclear spin pair under magic-angle spinning in solid-state NMR, J. Chem. Phys. 146 (2017).
[46] V. Ladizhansky, S. Vega, Polarization transfer dynamics in Lee-Goldburg cross polarization nuclear magnetic resonance experiments on rotating solids, J. Chem. Phys. 112 (2000) 7158–7168.
[47] M. Bjerring, N.C. Nielsen, Solid-state NMR heteronuclear coherence transfer using phase and amplitude modulated rf irradiation at the Hartmann-Hahn sideband conditions, Chem. Phys. Lett. 382 (2003) 671–678.
[48] S.V. Dvinskikh, H. Zimmermann, A. Maliniak, D. Sandström, Heteronuclear dipolar recoupling in solid-state nuclear magnetic resonance by amplitude-, phase-, and frequency-modulated Lee-Goldburg cross-polarization, J. Chem. Phys. 122 (2005).
[49] Z. Zhang, R. Fu, J. Li, J. Yang, Asymmetric simultaneous phase-inversion cross-polarization in solid-state MAS NMR: Relaxing selective polarization transfer condition between two dilute spins, J. Magn. Reson. 242 (2014) 214–219.
[50] W.K. Peng, K. Takeda, M. Kitagawa, A new technique for cross polarization in solid-state NMR compatible with high spinning frequencies and high magnetic fields, Chem. Phys. Lett. 417 (2006) 58–62.
[51] S. Wi, R. Schurko, L. Frydman, 1H–2H cross-polarization NMR in fast spinning solids by adiabatic sweeps, J. Chem. Phys. 146 (2017).
[52] P. Duan, K. Schmidt-Rohr, Composite-pulse and partially dipolar dephased multiCP for improved quantitative solid-state 13C NMR, J. Magn. Reson. 285 (2017) 68–78.
[53] T. Matsunaga, I. Matsuda, T. Yamazaki, Y. Ishii, Decoherence optimized tilted-angle cross polarization: A novel concept for sensitivity-enhanced solid-state NMR using ultra-fast magic angle spinning, J. Magn. Reson. 322 (2021).
[54] S.C. Shekar, W. Zhao, T.K. Weldeghiorghis, T. Wang, Effect of cross polarization radiofrequency phases on signal phase, Solid State Nucl. Magn. Reson. 117 (2022).
[55] A.C. Kolbert, S.L. Gann, Variable-effective-field cross polarization. An approach to broadband Hartmann-Hahn matching in MAS NMR, Chem. Phys. Lett. 224 (1994) 86–90.
[56] S. Jain, M. Bjerring, N.C. Nielsen, Efficient and Robust Heteronuclear Cross-Polarization for High-Speed-Spinning Biological Solid-State NMR Spectroscopy, J. Phys. Chem. Lett. 3 (2012) 703–708.
[57] K. Basse, S.K. Jain, O. Bakharev, N.C. Nielsen, Efficient polarization transfer between spin-1/2 and 14N nuclei in solid-state MAS NMR spectroscopy, J. Magn. Reson. 244 (2014) 85–89.
[58] A.B. Nielsen et al., Theoretical description of RESPIRATION-CP, Chem. Phys. Lett. 645 (2016) 150–156.
[59] J. Blahut, M.J. Brandl, T. Pradhan, B. Reif, Z. Tošner, Sensitivity-enhanced multidimensional solid-state NMR spectroscopy by optimal-control-based transverse mixing sequences, J. Am. Chem. Soc. (2022).
[60] Z. Tošner, M.J. Brandl, J. Blahut, S.J. Glaser, B. Reif, Maximizing efficiency of dipolar recoupling in solid-state NMR using optimal control sequences, Sci. Adv. 7 (2021) eabj5913.
[61] X. Zhao, M. Edén, M.H. Levitt, Recoupling of heteronuclear dipolar interactions in solid-state NMR using symmetry-based pulse sequences, Chem. Phys. Lett. 342 (2001) 353–361.
[62] R. Pratima, K.V. Ramanathan, Synchronous accumulation of polarisation. A new approach to cross polarisation under fast magic angle spinning, Chem. Phys. Lett. 221 (1994) 322–326.
[63] J. Raya, B. Perrone, J. Hirschinger, Chemical shift powder spectra enhanced by multiple-contact cross-polarization under slow magic-angle spinning, J. Magn. Reson. 227 (2013) 93–102.
[64] T. Kamihara, M. Murakami, Y. Noda, K. Takeda, K. Takegoshi, COMPOZER-based longitudinal cross-polarization via dipolar coupling under MAS, J. Magn. Reson. 245 (2014) 94–97.
[65] A.E. Bryson, Applied Optimal Control: Optimization, Estimation, and Control, Routledge, 2017, 10.1201/9781315137667.
[66] S.J. Glaser et al., Training Schrödinger's cat: quantum optimal control, Eur. Phys. J. D 69 (2015) 279.
[67] N.C. Nielsen, C. Kehlet, S.J. Glaser, N. Khaneja, Optimal Control Methods in NMR Spectroscopy, in: In *eMagRes*, John Wiley & Sons Ltd, 2010.
[68] N. Khaneja, T. Reiss, C. Kehlet, T. Schulte-Herbrüggen, S.J. Glaser, Optimal control of coupled spin dynamics: design of NMR pulse sequences by gradient ascent algorithms, J. Magn. Reson. 172 (2005) 296–305.
[69] Z. Zhang, J. Li, Y. Chen, H. Xie, J. Yang, A robust heteronuclear dipolar recoupling method comparable to TEDOR for proteins in magic-angle spinning solid-state NMR, J. Magn. Reson. 285 (2017) 79–85.
[70] S. Hediger, B.H. Meier, R.R. Ernst, Cross polarization under fast magic angle sample spinning using amplitude-modulated spin-lock sequences, Chem. Phys. Lett. 213 (1993) 627–635.
[71] X.L. Wu, K.W. Zilm, Cross Polarization with High-Speed Magic-Angle Spinning, J. Magn. Reson. A 104 (1993) 154–165.
[72] T.M. Barbara, E.H. Williams, Modulated sequences for cross polarization during high-speed MAS, J. Magn. Reson. 1969 (99) (1992) 439–442.
[73] M.H. Levitt, Heteronuclear cross polarization in liquid-state nuclear magnetic resonance: Mismatch compensation and relaxation behavior, J. Chem. Phys. 94 (1991) 30–38.
[74] S. Vega, Fictitious spin 1/2 operator formalism for multiple quantum NMR, J. Chem. Phys. 68 (1978) 5518–5527.
[75] M.M. Maricq, Application of average Hamiltonian theory to the NMR of solids, Phys. Rev. B 25 (1982) 6622–6632.
[76] S. Hediger, B.H. Meier, R.R. Ernst, Rotor-synchronized amplitude-modulated nuclear magnetic resonance spin-lock sequences for improved cross polarization under fast magic angle sample spinning, J. Chem. Phys. 102 (1995) 4000–4011.
[77] S. Hediger, P. Signer, M. Tomaselli, R.R. Ernst, B.H. Meier, A Combination of Slow and Fast RF Field Modulation for Improved Cross Polarization in Solid-State MAS NMR, J. Magn. Reson. 125 (1997) 291–301.
[78] M. Mehring, Principles of High Resolution NMR in Solids, Springer-Verlag, 1983, 10.1007/978-3-642-68756-3.
[79] U. Haeberlen, J.S. Waugh, Coherent Averaging Effects in Magnetic Resonance, Phys. Rev. 175 (1968) 453–467.
[80] E.T. Olejniczak, S. Vega, R.G. Griffin, Multiple pulse NMR in rotating solids, J. Chem. Phys. 81 (1984) 4804–4817.
[81] J. Zhou, C. Ye, A novel disentangling technique for the propagator describing cross-polarization dynamics, Solid State Nucl. Magn. Reson. 5 (1995) 213–216.
[82] G. Bodenhausen, R. Freeman, G.A. Morris, A simple pulse sequence for selective excitation in Fourier transform NMR, J. Magn. Reson. 1969 (23) (1976) 171–175.
[83] P. Caravatti, G. Bodenhausen, R.R. Ernst, Selective pulse experiments in high-resolution solid state NMR, J. Magn. Reson. 1969 (55) (1983) 88–103.
[84] I. Scholz, B.H. Meier, M. Ernst, Operator-based triple-mode Floquet theory in solid-state NMR, J. Chem. Phys. 127 (2007).
[85] A. Lange, I. Scholz, T. Manolikas, M. Ernst, B.H. Meier, Low-power cross polarization in fast magic-angle spinning NMR experiments, Chem. Phys. Lett. 468 (2009) 100–105.
[86] A.B. Nielsen, S. Jain, M. Ernst, B.H. Meier, N.C. Nielsen, Adiabatic rotor-echo-short-pulse-irradiation mediated cross-polarization, J. Magn. Reson. 237 (2013) 147–151.
[87] S. Laage et al., Band-Selective 1H–13C cross-polarization in fast magic angle spinning solid-state NMR spectroscopy, J. Am. Chem. Soc. 130 (2008) 17216–17217.